

Published in final edited form as:

Neuroimage. 2012 January 2; 59(1): 193–201. doi:10.1016/j.neuroimage.2011.07.034.

Hyperpolarized ^{13}C MR spectroscopic imaging can be used to monitor Everolimus treatment *in vivo* in an orthotopic rodent model of glioblastoma

Myriam M. Chaumeil^a, Tomoko Ozawa^b, IlWoo Park^a, Kristen Scott^a, C. David James^b, Sarah J. Nelson^a, and Sabrina M. Ronen^a

Myriam M. Chaumeil: myriam.chaumeil@ucsf.edu; Tomoko Ozawa: tomoko.ozawa@ucsf.edu; IlWoo Park: ilwoo.park@ucsf.edu; Kristen Scott: kristen.scott@ucsf.edu; C. David James: david.james@ucsf.edu; Sarah J. Nelson: sarah.nelson@ucsf.edu; Sabrina M. Ronen: sabrina.ronen@ucsf.edu

^aDepartment of Radiology and Biomedical Imaging, University of California San Francisco, 1700 4th Street Box 2532, San Francisco 94158, CA, USA

^bDepartment of Neurological Surgery, Brain Tumor Research Center, University of California San Francisco, Box 0520, San Francisco, CA 94143, CA, USA

Abstract

Glioblastoma (GBM) is the most common and lethal primary malignant brain tumor in humans. Because the phosphatidylinositol-3-kinase (PI3K) signaling pathway is activated in more than 88% of GBM, new drugs which target this pathway, such as the mTOR inhibitor Everolimus, are currently in clinical trials. Early tumor response to molecularly targeted treatments remains challenging to assess non-invasively, because it is often associated with tumor stasis or slower tumor growth. Innovative neuroimaging methods are therefore critically needed to provide metabolic or functional information that is indicative of targeted therapeutic action at early time points during the course of treatment.

In this study, we demonstrated for the first time that hyperpolarized (HP) ^{13}C magnetic resonance spectroscopic imaging (MRSI) can be used on a clinical MR system to monitor early metabolic response of orthotopic GBM tumors to Everolimus treatment through measurement of the HP lactate-to-pyruvate ratios. The study was performed on a highly invasive non-enhancing orthotopic GBM tumor model in rats (GS-2 tumors), which replicates many fundamental features of human GBM tumors. Seven days after initiation of treatment there was a significant drop in the HP lactate-to-pyruvate ratio from the tumor tissue in treated animals relative to day 0 ($67\% \pm 27\%$ decrease). In the control group, no significant changes in the HP lactate-to-pyruvate ratios were observed. Importantly, at the 7 day time point, conventional MR imaging (MRI) was unable to detect a significant difference in tumor size between control and treated groups. Inhibition of tumor growth by conventional MRI was observed from day 15 of treatment. This implies that the decrease in the HP lactate-to-pyruvate ratio could be detected before any treatment-induced inhibition of tumor growth.

Using immunohistochemical staining to further examine tumor response to treatment, we found that the decrease in the HP lactate-to-pyruvate ratio was associated with a drop in expression of lactate dehydrogenase, the enzyme that catalyzes pyruvate to lactate conversion. Also evident was

Corresponding author: Sabrina M. Ronen, Ph.D., 1700 4th Street, Box 2532, Byers Hall 3rd Floor, Suite, University of California, San Francisco, San Francisco, CA 94158, sabrina.ronen@ucsf.edu, Phone: 415-514-4839, Fax: 415-514-2550.

Publisher's Disclaimer: This is a PDF file of an unedited manuscript that has been accepted for publication. As a service to our customers we are providing this early version of the manuscript. The manuscript will undergo copyediting, typesetting, and review of the resulting proof before it is published in its final citable form. Please note that during the production process errors may be discovered which could affect the content, and all legal disclaimers that apply to the journal pertain.

decreased staining for carbonic anhydrase IX (CA-IX), an indicator of hypoxia-inducible factor 1 α (HIF-1 α) activity, which, in turn, regulates expression of lactate dehydrogenase.

To our knowledge, this study is the first report of the use of HP ^{13}C MRSI at a clinical field strength to monitor GBM response to molecularly targeted treatments. It highlights the potential of HP lactate-to-pyruvate ratio as an early biomarker of response, thereby supporting further investigation of this non-invasive imaging approach for eventual clinical application.

Keywords

Glioblastoma; Everolimus; mTOR inhibition; hyperpolarization; carbon 13 ^{13}C ; MRSI

1. INTRODUCTION

Between 2004 and 2006, more than 158,000 new cases of primary brain and central nervous system tumors were diagnosed in the United States, corresponding to an overall incidence of 18.71 per 100,000 people per year (CBRTUS, 2010). More than 27,000 of these tumors were classified as glioblastoma (GBM), which is the most common and aggressive type of primary brain tumor (Louis, 2007). The conventional care for patients diagnosed with GBM is based on the combination of maximal safe surgical resection with chemotherapy and radiotherapy treatments (Belda-Iniesta, 2008; Clarke, 2010; Stupp, 2009; Stupp, 2005; Stupp, 2010). Despite the use of adjuvant radiation and chemotherapy, tumor recurrence is observed in nearly all instances, and the median survival for GBM patients has seen only modest improvement, to approximately 15 months (CBRTUS, 2010). The identification of treatments that effectively and specifically target GBM for achieving improved patient outcomes remains an elusive goal.

A promising approach for the treatment of GBM is based on using molecularly targeted agents, i.e. new drugs specifically inhibiting a step in one of the many signaling pathways deregulated in cancer. The phosphatidylinositol-3-kinase (PI3K) signaling pathway, which plays a crucial role in cell growth, proliferation, differentiation, metabolism and survival, is activated in more than 88% of GBM (Bunney and Katan, 2010; CGARN, 2008).

Accordingly, new drugs that specifically target one or several steps in this pathway are currently being developed and evaluated (Cleary and Shapiro, 2010; Minniti, 2009; Workman, 2006). Among the possible targets, the mammalian target of rapamycin (mTOR) appears promising (Akhavan, 2010). Several mTOR inhibitors have been developed and several are being evaluated in clinical trials (Cleary and Shapiro, 2010). In particular, the anticancer drug Everolimus (RAD001), a rapamycin analog mTOR inhibitor, is currently being investigated for efficacy as a part of combination therapies in phase I/II clinical trials for newly diagnosed and recurrent GBM (Nguyen, 2006; Sarkaria, 2010) (<http://clinicaltrials.gov/>).

The assessment of early response to targeted therapies using conventional imaging methods such as magnetic resonance imaging (MRI) or computerized axial tomography (CT) remains a challenge. MRI and CT are mostly limited to the detection of anatomical changes, which typically occur at late time points post treatment initiation. These changes can be as drastic as tumor shrinkage, but treatment can also induce tumor stasis or inhibition of tumor growth. In such cases, anatomical imaging methods are unable to provide an early indication of tumor responsiveness to molecularly targeted treatments.

As a result of conventional imaging limitations, alternative neuroimaging methods are being developed and evaluated. Considering its high sensitivity to the intrinsic structural properties of biological tissues, diffusion-based MR imaging presents a promising alternative

neuroimaging approach for the study of GBM. Indeed methods such as diffusion-weighted imaging (DWI) and diffusion tensor imaging (DTI) have proven useful for patient stratification, diagnosis and prognosis (Byrnes, 2011; Ellingson, 2011; Pope, 2011; Saksena, 2010). However, these methods are only sensitive to structural variations, and cannot inform on tissue function. Neuroimaging methods aiming at measuring functional parameters associated with brain tumor metabolism are therefore being investigated based on the hypothesis that modulations of tumor metabolism occur at early stages post treatment initiation. In many cancer types, [^{18}F] 2-fluoro-2-deoxy-D-glucose positron emission tomography (FDG-PET) has shown great potential for monitoring response to therapy by exploiting the well-known increase in glucose uptake in tumors (Warburg, 1956). Unfortunately, this method presents several limitations for the study of GBM, with the most significant being that the high level of glucose uptake in tumors is hard to separate from the normally high background uptake in surrounding normal brain tissue (Phelps and Mazziotta, 1985). More recently, PET imaging of cellular proliferation using [^{18}F] fluorothymidine (FLT-PET) was shown as a promising approach to monitor treatment, both in preclinical models (Monazzam, 2009; Wei, 2008) and in clinical studies (Chen, 2007b). However, repeated longitudinal studies using PET imaging could be limited by radiation exposure.

^{13}C MR spectroscopy (MRS) or spectroscopic imaging (MRSI) in combination with the recently developed dynamic nuclear polarization technique (DNP) is a highly promising radiation free imaging method which, through the hyperpolarization of ^{13}C -labeled compounds, improves the MR detectable signal-to-noise ratio by a factor of 10,000 (Ardenkjaer-Larsen, 2003). As a consequence, ^{13}C MRS and ^{13}C MRSI of hyperpolarized (HP) probes have enabled non-invasive assessment of changes in several metabolic reactions (Viale and Aime, 2010).

Among the MRS probes, [$1\text{-}^{13}\text{C}$] pyruvate has been the most commonly used, as it fulfills the main requirements of a useful MR probe: (i) a long enough longitudinal relaxation time T_1 that enables monitoring of HP [$1\text{-}^{13}\text{C}$] pyruvate conversion into other HP species within the hyperpolarization lifetime, (ii) a high level of polarization providing adequate signal to noise for detection of substrate and product, and (iii) a high biological relevance due to its key role in metabolism. HP [$1\text{-}^{13}\text{C}$] pyruvate is extremely valuable for the study of cancer because the conversion of pyruvate into lactate, which is catalyzed by the enzyme lactate dehydrogenase (LDH), is abnormally elevated in tumor cells (Warburg, 1956). The use of HP [$1\text{-}^{13}\text{C}$] pyruvate has allowed assessment of tumor metabolism by monitoring its conversion to HP [$1\text{-}^{13}\text{C}$] lactate in preclinical models of cancer (Albers, 2008; Chen, 2007a; Day, 2007; Golman, 2006; Hu, 2010; Witney, 2009), including GBM (Park, 2010; Ward, 2010). Following these promising preclinical studies, a pioneer clinical trial using HP [$1\text{-}^{13}\text{C}$] pyruvate in prostate cancer patients is now ongoing at the University of California, San Francisco.

Recently, we demonstrated that ^{13}C MRS and ^{13}C MRSI of HP [$1\text{-}^{13}\text{C}$] pyruvate could be used to assess tumor response to molecularly targeted inhibition of the PI3K/mTOR signaling pathway by Everolimus in perfused GBM cells and in subcutaneous (sc) GBM tumors (Ward, 2010). Specifically, we showed that PI3K/mTOR inhibition resulted in a decrease in the conversion of HP [$1\text{-}^{13}\text{C}$] pyruvate into HP [$1\text{-}^{13}\text{C}$] lactate, and that this decrease was due to a drop in expression of the LDH isoform LDH-A, which, in turn, is likely due to a drop in expression of the mTOR regulated hypoxia-inducible factor 1α (HIF- 1α) transcription factor (Firth, 1995; Pouyssegur, 2006; Ward, 2010). In the present study we have further investigated the potential utility of ^{13}C MRSI of HP [$1\text{-}^{13}\text{C}$] pyruvate for studying GBM response to mTOR targeted inhibitor therapy, but in the context of the more relevant pre-clinical model involving invasive orthotopic (intracranial) GBM xenografts. Using HP ^{13}C MRSI on a clinically relevant 3T MR system, we demonstrate the

ability to non-invasively monitor orthotopic tumor mTOR inhibition by Everolimus, thus showing the potential of HP ^{13}C MRSI for assessing early brain tumor response to molecularly targeted therapies.

2. MATERIAL and METHODS

2.1. Cell culture

GS-2 cancer cells modified for bioluminescence imaging (BLI) via transduction with a firefly luciferase-encoding HIV1-based lentivirus (Gunther, 2008; Sarkaria, 2007) were kindly provided by Dr. Haas-Kogan and Dr. James (University of California, San Francisco). Cells were cultured in McCoy's medium supplemented with 10% heat-inactivated fetal bovine serum, 100units.mL⁻¹ penicillin and 100µg.mL⁻¹ streptomycin. They were maintained as exponentially growing monolayers at 37°C in a humidified atmosphere consisting of 95% air and 5% CO₂.

2.2. Intracranial injection of tumor cells

All animal research was approved by the Institutional Animal Care and Use Committee of the University of California, San Francisco. A total of nine male athymic rats (median weight 200g, rnu/rnu, homozygous) purchased from Harlan (Indianapolis, IN) were housed and fed under aseptic conditions. An hour before starting the intracranial (ic) injection, GS-2 BLI cells were washed once with phosphate buffered saline solution, harvested by trypsinization, counted and resuspended in serum-free McCoy's medium to a final concentration of 3×10^5 cells per 10µL. For ic injection, rats (5 to 6 week-old at the time of injection) were anesthetized by an intraperitoneal (ip) injection of a mixture of ketamine/xylazine (60/7.5mg.kg⁻¹ respectively). A volume of 10µL of cell suspension was slowly injected into the right caudate-putamen of the animal brain by free hand technique, as previously described (Ozawa, 2006; Ozawa, 2002). Buprenorphine was injected subcutaneously right after injection of tumor cells for optimal pain management (0.05mg.kg⁻¹, v=1mL).

2.3. Bioluminescence imaging

30±0.5 days post ic injection of tumor cells, BLI was performed to confirm intracranial tumor growth. Briefly, rats were anesthetized using isoflurane in O₂ (2%, 1.5mL.min⁻¹) and injected ip with a volume of 1mL luciferin at a dose of 150mg.kg⁻¹. The animals were then positioned in a cooled CCD camera (IVIS-200; Xenogen) and the presence of fluorescence from the tumor was assessed using the Living Image 2.5 software package (Xenogen).

2.4. Everolimus treatment

40±4 days post ic injection of tumor cells, treated animals (n=5) received a daily ip injection of Everolimus (10mg.kg⁻¹.day⁻¹ in DMSO, v=200µL, Molcan Corporation, Canada) while control animals (n=4) received the same volume of DMSO only. Seven days post initiation of treatment, 3 animals in each group were euthanized for further histological studies. Treatment with Everolimus/carrier was pursued on three animals (n=2 treated, n=1 control) for 23 days in order to confirm the long-term effects of treatment.

2.5. Animal handling during MR acquisitions

Prior to each experiment, animals were anesthetized using a mixture of isoflurane in O₂ (3%, 1.5mL.min⁻¹) then placed on an electric heating pad and maintained under anesthesia using a nose cone (1%-2% isoflurane in O₂, 1.5mL.min⁻¹) during catheter placement and throughout the imaging session. A 24G catheter was placed and secured into the tail vein of the animals to allow for intravenous (iv) injection of HP [1- ^{13}C] pyruvate. Rats were then

placed in a custom-made cradle allowing positioning of the brain in the center of the RF coil and in the center of the magnet. A water-heating pad placed under the animal was used to maintain stable body temperature throughout the imaging session.

2.6. Polarization and injection procedures

A volume of approximately 32 μ L (weight 45 \pm 1mg) of [1- 13 C] pyruvic acid (Isotech, Miamisburg, OH), 15mM OX63 trityl radical (Oxford Instruments, Abingdon, UK) and 0.5mM Dotarem (Gd-DOTA, Guerbet, France) was hyperpolarized using a HyperSense DNP polarizer (Oxford Instruments, Abingdon, UK) for approximately 1 hour (Ardenkjaer-Larsen, 2003; Park, 2010). The small quantity of Gd $^{3+}$ mixed in the preparation is used to increase the level of hyperpolarization of the [1- 13 C] pyruvic acid, as previously reported (Johannesson, 2009). At the end of the irradiation, HP [1- 13 C] pyruvic acid was rapidly dissolved in a 5.5 \pm 0.5mL volume of saline solution (40mM Tris, 100mM NaOH and 0.1mg.L $^{-1}$ Na $_2$ EDTA) in order to obtain a solution of 100mM buffered HP [1- 13 C] pyruvate. Within approximately 10 seconds after dissolution, a volume of 3.3 \pm 0.3mL of the 100mM buffered HP [1- 13 C] pyruvate solution was injected over 10 seconds by free hand in the tail vein of the animal through the previously placed catheter. The injection volume was adjusted to the animal's body weight in each experiment in order to achieve a final injected dose of HP [1- 13 C] pyruvate of 30mM per 100g of body weight. The 3D 13 C MRSI sequence was started 20 seconds after the beginning of the injection of HP pyruvate. This delay between injection and acquisition corresponds to the time of maximum lactate formation, as previously described (Park, 2010). The pH of the HP [1- 13 C] pyruvate solution measured post injection was in the physiological range for each experiment (pH=7.29 \pm 0.72).

2.7. 1 H and 13 C MR acquisitions

Experiments were performed on a 3T GE Signa $^{\text{TM}}$ system (GE Healthcare, Milwaukee, WI) equipped with a custom-designed dual-tuned 1 H- 13 C coil (quadrature 13 C channel, linear 1 H channel, 8cm inner coil diameter, 9cm length). Each animal underwent three MR sessions: one prior to Everolimus/carrier treatment (D0), one two days (D2) and one seven days (D7) post initiation of Everolimus/carrier treatment. Each of these MR sessions consisted of four steps: (i) acquisition of high-resolution T2-weighted anatomical images in the three imaging planes, (ii) iv injection of HP [1- 13 C] pyruvate, (iii) acquisition of the 13 C 3D MRSI data and (iv) acquisition of axial contrast enhanced T1-weighted images. Three animals (n=2 treated, n=1 control) were also imaged at day 9, 15 and 23 days in order to confirm the long-term effects of treatment (T2-weighted and T1-weighted MR imaging only, no 13 C 3D MRSI).

T2-weighted anatomical images were acquired using a fast spin-echo (FSE) sequence in all three imaging planes (TE/TR=60/4000ms) using a field of view of 8cm (axial: 320 \times 192 matrix, 2mm slice thickness, 5 NEX; sagittal: 256 \times 192 matrix, 2mm slice thickness, 4 NEX; coronal: 256 \times 192 matrix, 1.5mm slice thickness, 4 NEX). These images were used to assess the tumor size and location and to reproducibly position the 13 C 3D MRSI grid based upon anatomical landmarks. A previously described double spin echo (SE) sequence was used to acquire the 13 C 3D MRSI data 20 seconds post iv injection of HP [1- 13 C] pyruvate (TE/TR=140/215ms, 4 \times 4 \times 5.4mm resolution, centric k-space encoding, variable flip angle scheme, 17seconds acquisition time) (Cunningham, 2007). After acquisition of the HP 13 C data, 0.1 mL Magnevist (Gd-DTPA, Bayer Schering, 0.2 mmol.kg $^{-1}$) was injected and axial contrast enhanced T1-weighted SE images were acquired with the following parameters: TE/TR=10/700 ms, 8cm FOV, 320 \times 192 matrix, 1.2mm slice thickness 6 NEX.

2.8. Data post-processing and analysis

Tumor volume was assessed from the anatomical T2-weighted images using dedicated in-house software (Nelson, 2001). Briefly, for each animal at each time point, manual contouring of the tumor was performed in each axial slice, defining the vertices of the tumor region in real coordinates. The final volume was then calculated as the sum throughout slices of the tumor region area times the slice thickness.

All HP ^{13}C 3D MRSI data were post processed using in-house software, as previously described (Nelson, 2001). Superimposition of the 3D ^{13}C MRSI data on the axial T2-weighted images was performed in order to localize the central tumor voxel (>80% of tumor tissue) for each MR experiment. For each of the three imaging time points (D_i with $i=0, 2$ and 7 days of Everolimus treatment), the magnitude spectrum from the tumor voxel was used to assess the integrals of the lactate and pyruvate peaks and calculate the lactate-to-pyruvate ratio $(Lactate/Pyruvate)_{D_i}^{TUMOR}$. Integral values of lactate and pyruvate signals were also estimated from a contralateral voxel, symmetrical with the tumor voxel relative to the midsagittal line, in order to assess the normal brain lactate-to-pyruvate ratio $(Lactate/Pyruvate)_{D_i}^{CONTRALATERAL}$. The values of the tumor lactate-to-pyruvate ratios normalized to the values of this ratio in the contralateral brain were calculated for each animal and for the three imaging time points (D_i with $i=0, 2$ and 7) as follows:

$$(Lactate/Pyruvate)_{D_i} = \frac{(Lactate/Pyruvate)_{D_i}^{TUMOR}}{(Lactate/Pyruvate)_{D_i}^{CONTRALATERAL}}$$

In order to assess the variations of this ratio during Everolimus treatment, the values of this ratio were expressed as a percentage of the $(Lactate/Pyruvate)_{D_0}$ measured prior to treatment initiation (D_0), as follows:

$$(Lactate/Pyruvate)_{D_{0,2,7}}^{NORMALIZED} = \frac{(Lactate/Pyruvate)_{D_{0,2,7}}}{(Lactate/Pyruvate)_{D_0}} \times 100$$

The final ratios $(Lactate/Pyruvate)_{D_{0,2,7}}^{NORMALIZED}$ were then averaged within the animal groups (control and treated). A heatmap of this ratio was generated by spatial interpolation of the processed ^{13}C MRSI data to the resolution of the anatomical image.

2.9. Statistical analysis

A two-tailed paired Student's t-test was used to verify the statistical significance of differences between time points within each group, and a two-tailed unpaired t-test was used to assess the significance of differences between groups at each time point. All results are expressed as mean \pm sd and $p \leq 0.05$ was considered significant.

2.10. Immunohistochemistry (IHC)

At D7 after initiation of treatment, animals (n=3 controls, n=3 treated) were euthanized, their brains resected and placed in 10% buffered formalin for 24 hours. The brains were embedded in paraffin and sectioned in the axial plane. The following IHC stains were performed by the UCSF Tissue core: hematoxylin and eosin (H&E, HXHHEGAL/STE0157 antibody, American Mastertech Scientific), carbonic anhydrase IX (CA-IX, NB100-417 antibody, Novus Biologicals), factor VIII (FVIII, A0082 antibody, Dako), mindbomb homolog 1 (MIB-1, 790-4286 antibody, Ventana), caspase 3 (Casp3, 9661 antibody, Cell signaling) and lactate dehydrogenase A (LDH-A, 1980-1 antibody, Epitomics).

All stained slides were imaged using a Nikon Eclipse Ti-E motorized inverted microscope (Nikon Imaging Center, University of California, San Francisco) and assessed qualitatively.

3. RESULTS

3.1. Everolimus treatment does not induce a detectable effect on tumor growth after seven days of treatment, as assessed by conventional MR imaging

BLI of luciferase-modified intracranial GS-2 xenografts was performed prior to starting the MR imaging sessions in order to confirm the presence of intracranial tumor. Detectable GS-2 tumor developed in all nine animals 30 ± 0.5 days post ic injection (data not shown). Tumors were allowed to progress until day 40 ± 4 to achieve sufficient volume for MR spectroscopic imaging. At this time, tumors were visible as areas of hypersignal on T2-weighted images, as shown in Figure 1A. The dotted lines superimposed to anatomical images highlight tumor areas between D0 and D7 for one control and one treated animal. Contrast enhanced T1-weighted images show no enhancement in the tumor region, confirming the invasive non-enhancing feature of this tumor model (data not shown).

Figure 1B shows the tumor growth curves as a function of days following treatment initiation for the control and treated groups. Tumor volumes were significantly increased compared to pre-treatment following 7 days of Everolimus or carrier ($223 \pm 9\%$ of D0 for treated, $p = 8 \times 10^{-6}$ and $250 \pm 25\%$ of D0 for controls, $p = 0.001$), consistent with the representative images in Figure 1A. The differences in tumor volume between the two groups were not significant at D2 ($p = 0.5$) or D7 ($p = 0.1$) but were detected by day 15 (D15) of treatment ($n = 1$ control, $n = 2$ treated). Even though no statistical analysis regarding the difference in tumor volumes could be derived from D15 data due to the limited number of animals, this single case observation is in agreement with the known anti-tumor effect of Everolimus administration (Goudar, 2005; Yang, 2008).

3.2. HP lactate-to-pyruvate ratios reveal differences in tumor metabolism between treated and control animals

HP ^{13}C MRSI and anatomical imaging were performed at D0, D2 and D7 post initiation of treatment. Figure 2 presents MR datasets obtained at D0 and D7 for one of the Everolimus treated animals. HP [$1\text{-}^{13}\text{C}$] pyruvate is detectable in each voxel of the grid, and is comparable between normal brain and tumor. However, HP [$1\text{-}^{13}\text{C}$] lactate signal is much higher in the tumor region, as a result of the high glycolytic activity of GBM tumor cells.

Importantly, tumor HP ^{13}C spectra indicate a decrease in the $(\text{Lactate}/\text{Pyruvate})_{\text{D0,7}}^{\text{TUMOR}}$ ratio after 7 days of Everolimus treatment (Figure 2C).

Heatmaps of normalized $(\text{Lactate}/\text{Pyruvate})_{\text{D0,7}}^{\text{NORMALIZED}}$ values generated from HP ^{13}C MRSI datasets and corresponding anatomical images are presented in Figure 3, and illustrate both the spatial and temporal modulations in the $(\text{Lactate}/\text{Pyruvate})_{\text{D0,7}}^{\text{NORMALIZED}}$ values. These maps additionally show the close spatial correspondence between tumor tissues hypersignals on T2-weighted images (Figure 3A) and areas of high $(\text{Lactate}/\text{Pyruvate})_{\text{D0,7}}^{\text{NORMALIZED}}$ (Figure 3B), which decreases in the Everolimus treated animal after 7 days, in agreement with data presented in Figure 2. In contrast, this ratio increases after 7 days of control animal carrier treatment.

A histogram of the average $(\text{Lactate}/\text{Pyruvate})_{\text{D0,7}}^{\text{NORMALIZED}}$ values over time (D0, D2 and D7), for both control and treated groups, is presented in Figure 4. After 2 days, no significant difference was evident between Everolimus and control animals. However, after 7 days of treatment, the values of these ratios were significantly lower in treated vs. control

subjects ($p < 0.05$):

$(Lactate/Pyruvate)_{D7}^{NORMALIZED}$ (treated) = $67 \pm 27\%$, $(Lactate/Pyruvate)_{D7}^{NORMALIZED}$ (control) = $160 \pm 60\%$

From a clinical perspective it is more important to assess the potential of HP lactate-to-pyruvate ratios for longitudinal follow-up of treatment. The values of

$(Lactate/Pyruvate)_{D7}^{NORMALIZED}$ (treated) drop significantly in treated animals within 7 days of Everolimus treatment ($p < 0.05$):

$(Lactate/Pyruvate)_{D0}^{NORMALIZED}$ (treated) = $100 \pm 0\%$, $(Lactate/Pyruvate)_{D7}^{NORMALIZED}$ (treated) = $67 \pm 27\%$. In contrast, in the control group, these ratios showed an increasing trend but the changes were not statistically significantly ($p = 0.1$ at D7).

It is also important to note that the observed drop in $(Lactate/Pyruvate)_{D7}^{NORMALIZED}$ following treatment is specific to the tumor tissue and is not a general effect of Everolimus on the entire brain. Indeed, the values of $(Lactate/Pyruvate)^{TUMOR}$, when not normalized to the contralateral brain, follow the same trend. Furthermore, it is important to highlight that the values of $(Lactate/Pyruvate)^{CONTRALATERAL}$ remain stable throughout the 7 days of treatment, with no significant differences found between D0, D2 and D7 for both groups. More importantly, the values of $(Lactate/Pyruvate)^{CONTRALATERAL}$ are not significantly different between the two groups: the average value for all animals over D0, D2 and D7 was 0.40 ± 0.20 in the case of treated animals, and 0.44 ± 0.25 in the case of controls ($p = 0.7$). The rather high standard deviations on these values reflect the inter-animal intrinsic physiological variability and highlight the need for normalization to contralateral brain. This normalization provides a method for compensating for the small biological variations in levels of HP [$1-^{13}C$] pyruvate delivered to the brain and enhances the significance of results.

3.6. The decrease in lactate signal in the tumor reflects a decrease in LDH expression

We have previously shown that the drop in HP [$1-^{13}C$] pyruvate to HP [$1-^{13}C$] lactate conversion following inhibition of the PI3K/mTOR pathway is associated with a drop in LDH-A expression and activity in GBM perfused cells (Ward, 2010). In order to confirm this *in vivo*, IHC was performed on the tumors after 7 days of Everolimus vs. carrier treatment as shown in Figure 5. No changes in the levels of Casp3 could be detected between control and treated animals at D7, suggesting that the levels of apoptosis were highly similar between the two groups at that time point (Figure 5A). The level of proliferation, as shown by MIB-1 staining results in Figure 5B, as well as FVIII staining (data not shown) were also similar in the control and treated groups at D7. In contrast, Everolimus treatment induced a substantial decrease in the level of CA-IX relative to control animals, supporting decreased HIF-1 α levels following mTOR inhibition (Figure 5C) (Ward, 2010). A striking decrease in the expression of the enzyme that catalyzed the conversion of lactate to pyruvate, LDH-A, is also evident in Everolimus treated tumors as compared to control (Figure 5D).

4. DISCUSSION

Non-invasive assessment of early response to treatment is critical to achieving improved outcomes for GBM patients. In this study, we show that HP ^{13}C MRSI is a promising non-invasive neuroimaging technique that can provide early information on the metabolic status of tumors treated with the mTOR inhibitor Everolimus.

Conventional MR imaging was unable to detect changes in tumor volume in an orthotopic GBM xenograft model for up to 7 days of Everolimus treatment. This observation is in

agreement with the results in previous reports that indicate that sustained treatment is required for detecting Everolimus GBM anti-tumor effect in subcutaneous and orthotopic GBM models (Goudar, 2005; Yang, 2008).

In contrast, HP ^{13}C MRSI provided indication of Everolimus anti-tumor effect as early as 7 days post treatment initiation through the measurement of the lactate-to-pyruvate ratios $(\text{Lactate/Pyruvate})^{\text{NORMALIZED}}$. Moreover, analysis of the $(\text{Lactate/Pyruvate})^{\text{NORMALIZED}}$ values associated with longitudinal imaging of treated subjects indicates the potential of MRSI for indicating both extent and duration of inhibitor anti-tumor activity. Therefore, HP ^{13}C MRSI would not only identify early response to treatment, but could additionally be used to determine when patient tumors are acquiring resistance to therapy.

HP ^{13}C MRSI detects HP $[1-^{13}\text{C}]$ lactate levels originating from the conversion of exogenous HP $[1-^{13}\text{C}]$ pyruvate by the LDH enzyme in the tumor. As a consequence, the HP lactate-to-pyruvate ratio measured in the tumor tissue depends on (i) $[1-^{13}\text{C}]$ pyruvate delivery and transport to tumor cells, (ii) level of the LDH cofactor NADH and (iii) level of active LDH enzyme converting HP $[1-^{13}\text{C}]$ pyruvate into HP $[1-^{13}\text{C}]$ lactate. With regard to the former, it is important to emphasize that the orthotopic GS-2 tumor model used in this study was chosen because of its high invasiveness that should promote retention of an intact blood brain barrier (BBB). Indeed, contrast enhanced MR imaging studies of these tumors do not show any enhancement in the tumor region following injection of Gd-based contrast agent, even after a week of Everolimus treatment. Consistent with the MRI observations, analysis of FVIII and H&E IHC stains of GS-2 tumors shows that the density of blood capillaries is comparable between normal and tumor tissues after a week of Everolimus treatment, supporting vessel co-option by tumor, as previously described (di Tomaso, 2011; Leenders, 2002). Although minor alterations of the BBB affecting HP $[1-^{13}\text{C}]$ pyruvate delivery to tumor cannot be entirely discounted, the lack of Gd enhancement indicates that the extent to which the BBB is preserved in the GS-2 model is superior to that associated with non-invasive orthotopic GBM xenograft models, such as U87-MG.

Regarding the levels of NADH, cellular apoptotic response to treatment induces a depletion of the NADH pools, which could result in a drop in the level of HP $[1-^{13}\text{C}]$ lactate detected by ^{13}C MRSI (Day, 2007). However, results from IHC analysis of activated caspase 3 showed that the levels of apoptosis are low and comparable between control and treated groups at D7, thereby decreasing the likelihood of large variations in $(\text{Lactate/Pyruvate})^{\text{NORMALIZED}}$ NADH pool as contributing to observed differences in ratios between control and treated groups.

Whereas BBB disruption and cellular NADH levels do not appear to be affected by Everolimus treatment, decreased expression of LDH in association with Everolimus treatment was evident, and is likely a consequence of mTOR inhibition. Because the conversion of HP $[1-^{13}\text{C}]$ pyruvate into HP $[1-^{13}\text{C}]$ lactate is catalyzed by the LDH enzyme, a lower level of LDH expression in the Everolimus-treated tumors is likely to induce a decrease in $(\text{Lactate/Pyruvate})_{\text{D7}}^{\text{NORMALIZED}}$ (treated) measured by HP ^{13}C MRSI.

The added value of HP ^{13}C MRSI when comparing to anatomical MRI is clear. However it is important to address the relative advantages of HP ^{13}C MRSI compared to the already clinically available functional neuroimaging technique, FDG-PET. Results from a recent publication indicate that HP ^{13}C MRSI has comparable sensitivity for monitoring tumor response to etoposide in a murine lymphoma model (Witney, 2009). However, the effects of etoposide are primarily pro-apoptotic and result in decreased tumor cellularity, which, in turn, leads to a decrease in FDG uptake by the tumor. In the case of molecularly-targeted drugs such as Everolimus, which do not induce high levels of apoptosis, the ability of FDG-PET to

detect tumor changes is less certain. In fact, a recent phase I clinical trial of Everolimus and temozolomide in combination with radiation therapy in newly diagnosed GBM patients revealed that FDG uptake was unchanged in 14 out of 18 patients after one week of Everolimus treatment (Sarkaria, 2010). Furthermore, as mentioned previously, FDG-PET is often unable to detect variations in cerebral FDG-uptake in brain tumors, due to the high signal background coming from surrounding normal tissues. A further advantage of HP ^{13}C MRSI is associated with the use of a non-radioactive tracer. Currently, the main limitation of HP ^{13}C MRSI in comparison with FDG-PET is a lower spatial resolution. The resolution used in this study was $4\times 4\times 5.4\text{mm}$ as compared to the resolution of FDG-PET neuroimaging, which is in the range of 1.25–2mm isotropic. However, the resolution of HP ^{13}C MRSI is anticipated to experience rapid improvement in the very near future due to the development of new ultra fast neuroimaging sequences dedicated to the detection of hyperpolarized ^{13}C compounds (Larson, 2011; Tropp, 2011).

5. CONCLUSION

This study is the first report of the use of HP ^{13}C MRSI for monitoring molecularly targeted treatment in invasive non-enhancing GBM tumors at clinical field strength. The results described in this study confirm those we previously reported in treated cells and sc tumors. We showed that modulations of $(\text{Lactate/Pyruvate})^{\text{NORMALIZED}}$ ratios can be detected as early as 7 days post treatment initiation, even though no changes in tumor growth between control and Everolimus treated groups could be observed at that time point. This confirms our working hypothesis that changes in tumor metabolism induced by molecularly targeted treatment occur prior to any detectable changes in tumor size.

A clinical trial monitoring the use of HP ^{13}C MRSI is ongoing in prostate cancer patients at the University of California San Francisco with very promising preliminary results. The application of this technique for diagnosis and treatment follow-up of GBM patients is likely to be next. Our study shows encouraging results for the eventual clinical application of HP ^{13}C MRSI for assessing the extent of GBM patient tumor response to targeted small molecule inhibitor therapy. This, in turn, should facilitate improved clinical management of GBM through more rapid identification of efficacious therapies in treating individual tumors, and through longitudinal monitoring of tumor response to therapy, to identify a stage of treatment at which acquired resistance to therapy is indicated, allowing alternative treatments to be administered.

Acknowledgments

The authors would like to thank Humsa Venkatesh for help with cell culture. This work was supported by NIH UCSF Brain Tumor SPORE P50 CA097257, UC Discovery grants in conjunction with GE Healthcare, and NIH RO1 CA130819.

Abbreviations

GBM	glioblastoma
PI3K	phosphatidylinositol-3-kinase
mTOR	mammalian target of rapamycin
MRI	magnetic resonance imaging
CT	computerized axial tomography
FDG-PET	[^{18}F] 2-fluoro-2-deoxy-D-glucose positron emission tomography

MRS	magnetic resonance spectroscopy
MRSI	magnetic resonance spectroscopic imaging
DNP	dynamic nuclear polarization
HP	hyperpolarized
LDH	lactate dehydrogenase
HIF-1α	hypoxia-inducible factor 1 α
BLI	bioluminescence imaging
ic	intracranial
ip	intraperitoneal
FSE	fast spin-echo
FOV	field of view
NEX	number of excitations
SE	spin-echo
IHC	immunohistochemistry
H&E	hematoxylin and eosin
CA-IX	carbonic anhydrase IX
FVIII	factor VIII
MIB 1	mindbomb homolog 1
Casp3	caspase 3
NADH	nicotinamide adenine dinucleotide
BBBm	blood brain barrier

References

- Akhavan D, Cloughesy TF, Mischel PS. 2010 mTOR signaling in glioblastoma: lessons learned from bench to bedside. *Neuro Oncol.* 2010; 12(8):882–889. [PubMed: 20472883]
- Albers MJ, Bok R, Chen AP, Cunningham CH, Zierhut ML, Zhang VY, Kohler SJ, Tropp J, Hurd RE, Yen YF, Nelson SJ, Vigneron DB, Kurhanewicz J. 2008 Hyperpolarized ¹³C lactate, pyruvate, and alanine: noninvasive biomarkers for prostate cancer detection and grading. *Cancer Res.* 2008; 68(20):8607–8615. [PubMed: 18922937]
- Ardenkjaer-Larsen JH, Fridlund B, Gram A, Hansson G, Hansson L, Lerche MH, Servin R, Thaning M, Golman K. Increase in signal-to-noise ratio of > 10,000 times in liquid-state NMR. *Proc Natl Acad Sci U S A.* 2003; 100(18):10158–10163. [PubMed: 12930897]
- Belda-Iniesta C, de Castro Carpeno J, Sereno M, Gonzalez-Baron M, Perona R. Epidermal growth factor receptor and glioblastoma multiforme: molecular basis for a new approach. *Clin Transl Oncol.* 2008; 10(2):73–77. [PubMed: 18258505]
- Bunney TD, Katan M. Phosphoinositide signalling in cancer: beyond PI3K and PTEN. *Nat Rev Cancer.* 2010; 10(5):342–352. [PubMed: 20414202]
- Byrnes TJ, Barrick TR, Bell BA, Clark CA. Diffusion tensor imaging discriminates between glioblastoma and cerebral metastases in vivo. *NMR Biomed.* 2011; 24(1):54–60. [PubMed: 20665905]
- CBRTUS. Statistical report - Primary brain and central nervous system tumors diagnosed in the United states in 2004–2006. 2010. Available from: <http://seer.cancer.gov/>

- CGARN. Comprehensive genomic characterization defines human glioblastoma genes and core pathways. *Nature*. 2008; 455(7216):1061–1068. [PubMed: 18772890]
- Chen AP, Albers MJ, Cunningham CH, Kohler SJ, Yen YF, Hurd RE, Tropp J, Bok R, Pauly JM, Nelson SJ, Kurhanewicz J, Vigneron DB. Hyperpolarized C-13 spectroscopic imaging of the TRAMP mouse at 3T-initial experience. *Magn Reson Med*. 2007a; 58(6):1099–1106. [PubMed: 17969006]
- Chen W, Delaloye S, Silverman DH, Geist C, Czernin J, Sayre J, Satyamurthy N, Pope W, Lai A, Phelps ME, Cloughesy T. Predicting treatment response of malignant gliomas to bevacizumab and irinotecan by imaging proliferation with [18F] fluorothymidine positron emission tomography: a pilot study. *J Clin Oncol*. 2007b; 25(30):4714–4721. [PubMed: 17947718]
- Clarke J, Butowski N, Chang S. Recent advances in therapy for glioblastoma. *Arch Neurol*. 2010; 67(3):279–283. [PubMed: 20212224]
- Cleary JM, Shapiro GI. Development of phosphoinositide-3 kinase pathway inhibitors for advanced cancer. *Curr Oncol Rep*. 2010; 12(2):87–94. [PubMed: 20425592]
- Cunningham CH, Chen AP, Albers MJ, Kurhanewicz J, Hurd RE, Yen YF, Pauly JM, Nelson SJ, Vigneron DB. Double spin-echo sequence for rapid spectroscopic imaging of hyperpolarized ¹³C. *J Magn Reson*. 2007; 187(2):357–362. [PubMed: 17562376]
- Day SE, Kettunen MI, Gallagher FA, Hu DE, Lerche M, Wolber J, Golman K, Ardenkjaer-Larsen JH, Brindle KM. Detecting tumor response to treatment using hyperpolarized ¹³C magnetic resonance imaging and spectroscopy. *Nat Med*. 2007; 13(11):1382–1387. [PubMed: 17965722]
- di Tomaso E, Snuderl M, Kamoun WS, Duda DG, Auluck PK, Fazlollahi L, Andronesi OC, Frosch MP, Wen PY, Plotkin SR, Hedley-Whyte ET, Sorensen AG, Batchelor TT, Jain RK. Glioblastoma Recurrence after Cediranib Therapy in Patients: Lack of “Rebound” Revascularization as Mode of Escape. *Cancer Res*. 2011; 71(1):19–28. [PubMed: 21199795]
- Ellingson BM, Cloughesy TF, Lai A, Nghiemphu PL, Liao LM, Pope WB. High Order Diffusion Tensor Imaging in Human Glioblastoma. *Acad Radiol*. 2011:2011.
- Firth JD, Ebert BL, Ratcliffe PJ. Hypoxic regulation of lactate dehydrogenase A. Interaction between hypoxia-inducible factor 1 and cAMP response elements. *J Biol Chem*. 1995; 270(36):21021–21027. [PubMed: 7673128]
- Golman K, Zandt RI, Lerche M, Pehrson R, Ardenkjaer-Larsen JH. Metabolic imaging by hyperpolarized ¹³C magnetic resonance imaging for in vivo tumor diagnosis. *Cancer Res*. 2006; 66(22):10855–10860. [PubMed: 17108122]
- Goudar RK, Shi Q, Hjelmeland MD, Keir ST, McLendon RE, Wikstrand CJ, Reese ED, Conrad CA, Traxler P, Lane HA, Reardon DA, Cavenee WK, Wang XF, Bigner DD, Friedman HS, Rich JN. Combination therapy of inhibitors of epidermal growth factor receptor/vascular endothelial growth factor receptor 2 (AEE788) and the mammalian target of rapamycin (RAD001) offers improved glioblastoma tumor growth inhibition. *Mol Cancer Ther*. 2005; 4(1):101–112. [PubMed: 15657358]
- Gunther HS, Schmidt NO, Phillips HS, Kemming D, Kharbanda S, Soriano R, Modrusan Z, Meissner H, Westphal M, Lamszus K. Glioblastoma-derived stem cell-enriched cultures form distinct subgroups according to molecular and phenotypic criteria. *Oncogene*. 2008; 27(20):2897–2909. [PubMed: 18037961]
- Hu S, Lustig M, Balakrishnan A, Larson PE, Bok R, Kurhanewicz J, Nelson SJ, Goga A, Pauly JM, Vigneron DB. 3D compressed sensing for highly accelerated hyperpolarized (¹³C) MRSI with in vivo applications to transgenic mouse models of cancer. *Magn Reson Med*. 2010; 63(2):312–321. [PubMed: 20017160]
- Johannesson H, Macholl S, Ardenkjaer-Larsen JH. Dynamic Nuclear Polarization of [1-¹³C]pyruvic acid at 4.6 tesla. *J Magn Reson*. 2009; 197(2):167–175. [PubMed: 19162518]
- Larson PE, Hu S, Lustig M, Kerr AB, Nelson SJ, Kurhanewicz J, Pauly JM, Vigneron DB. Fast dynamic 3D MR spectroscopic imaging with compressed sensing and multiband excitation pulses for hyperpolarized (¹³C) studies. *Magn Reson Med*. 2011; 65(3):610–619. [PubMed: 20939089]
- Leenders WP, Kusters B, de Waal RM. Vessel co-option: how tumors obtain blood supply in the absence of sprouting angiogenesis. *Endothelium*. 2002; 9(2):83–87. [PubMed: 12200959]

- Louis DN, Ohgaki H, Wiestler OD, Cavenee WK, Burger PC, Jouvet A, Scheithauer BW, Kleihues P. The 2007 WHO classification of tumours of the central nervous system. *Acta Neuropathol.* 2007; 114(2):97–109. [PubMed: 17618441]
- Minniti G, Muni R, Lanzetta G, Marchetti P, Enrici RM. Chemotherapy for glioblastoma: current treatment and future perspectives for cytotoxic and targeted agents. *Anticancer Res.* 2009; 29(12): 5171–5184. [PubMed: 20044633]
- Monazzam A, Razifar P, Ide S, Rugaard Jensen M, Josephsson R, Blomqvist C, Langstrom B, Bergstrom M. Evaluation of the Hsp90 inhibitor NVP-AUY922 in multicellular tumour spheroids with respect to effects on growth and PET tracer uptake. *Nucl Med Biol.* 2009; 36(3):335–342. [PubMed: 19324279]
- Nelson SJ. Analysis of volume MRI and MR spectroscopic imaging data for the evaluation of patients with brain tumors. *Magn Reson Med.* 2001; 46(2):228–239. [PubMed: 11477625]
- Nguyen TD, Lassman AB, Lis E, Rosen N, Shaffer DR, Scher HI, Deangelis LM, Abrey LE. A pilot study to assess the tolerability and efficacy of RAD-001 (everolimus) with gefitinib in patients with recurrent glioblastoma multiforme (GBM). *Journal of Clinical Oncology.* 2006; 24(18S)
- Ozawa T, Faddegon BA, Hu LJ, Bollen AW, Lamborn KR, Deen DF. Response of intracerebral human glioblastoma xenografts to multifraction radiation exposures. *Int J Radiat Oncol Biol Phys.* 2006; 66(1):263–270. [PubMed: 16904526]
- Ozawa T, Wang J, Hu LJ, Bollen AW, Lamborn KR, Deen DF. Growth of human glioblastomas as xenografts in the brains of athymic rats. *In Vivo.* 2002; 16(1):55–60. [PubMed: 11980362]
- Park I, Larson PE, Zierhut ML, Hu S, Bok R, Ozawa T, Kurhanewicz J, Vigneron DB, Vandenberg SR, James CD, Nelson SJ. Hyperpolarized ¹³C magnetic resonance metabolic imaging: application to brain tumors. *Neuro Oncol.* 2010; 12(2):133–144. [PubMed: 20150380]
- Phelps ME, Mazziotta JC. Positron emission tomography: human brain function and biochemistry. *Science.* 1985; 228(4701):799–809. [PubMed: 2860723]
- Pope WB, Lai A, Mehta R, Kim HJ, Qiao J, Young JR, Xue X, Goldin J, Brown MS, Nghiemphu PL, Tran A, Cloughesy TF. Apparent diffusion coefficient histogram analysis stratifies progression-free survival in newly diagnosed bevacizumab-treated glioblastoma. *AJNR Am J Neuroradiol.* 2011; 32(5):882–889. [PubMed: 21330401]
- Pouyssegur J, Dayan F, Mazure NM. Hypoxia signalling in cancer and approaches to enforce tumour regression. *Nature.* 2006; 441(7092):437–443. [PubMed: 16724055]
- Saksena S, Jain R, Narang J, Scarpace L, Schultz LR, Lehman NL, Hearshen D, Patel SC, Mikkelsen T. Predicting survival in glioblastomas using diffusion tensor imaging metrics. *J Magn Reson Imaging.* 2010; 32(4):788–795. [PubMed: 20882608]
- Sarkaria JN, Galanis E, Wu W, Peller PJ, Giannini C, Brown PD, Uhm JH, McGraw S, Jaeckle KA, Buckner JC. North Central Cancer Treatment Group Phase I Trial N057K of Everolimus (RAD001) and Temozolomide in Combination with Radiation Therapy in Patients with Newly Diagnosed Glioblastoma Multiforme. *Int J Radiat Oncol Biol Phys.* 2010:2010.
- Sarkaria JN, Yang L, Grogan PT, Kitange GJ, Carlson BL, Schroeder MA, Galanis E, Giannini C, Wu W, Dinca EB, James CD. Identification of molecular characteristics correlated with glioblastoma sensitivity to EGFR kinase inhibition through use of an intracranial xenograft test panel. *Mol Cancer Ther.* 2007; 6(3):1167–1174. [PubMed: 17363510]
- Stupp R, Hegi ME, Mason WP, van den Bent MJ, Taphoorn MJ, Janzer RC, Ludwin SK, Allgeier A, Fisher B, Belanger K, Hau P, Brandes AA, Gijtenbeek J, Marosi C, Vecht CJ, Mokhtari K, Wesseling P, Villa S, Eisenhauer E, Gorlia T, Weller M, Lacombe D, Cairncross JG, Mirimanoff RO. Effects of radiotherapy with concomitant and adjuvant temozolomide versus radiotherapy alone on survival in glioblastoma in a randomised phase III study: 5-year analysis of the EORTC-NCIC trial. *Lancet Oncol.* 2009; 10(5):459–466. [PubMed: 19269895]
- Stupp R, Mason WP, van den Bent MJ, Weller M, Fisher B, Taphoorn MJ, Belanger K, Brandes AA, Marosi C, Bogdahn U, Curschmann J, Janzer RC, Ludwin SK, Gorlia T, Allgeier A, Lacombe D, Cairncross JG, Eisenhauer E, Mirimanoff RO. Radiotherapy plus concomitant and adjuvant temozolomide for glioblastoma. *N Engl J Med.* 2005; 352(10):987–996. [PubMed: 15758009]

- Stupp R, Tonn JC, Brada M, Pentheroudakis G. High-grade malignant glioma: ESMO Clinical Practice Guidelines for diagnosis, treatment and follow-up. *Ann Oncol.* 2010; 21 (Suppl 5):v190–193. [PubMed: 20555079]
- Tropp J, Lupo JM, Chen A, Calderon P, McCune D, Grafendorfer T, Ozturk-Isik E, Larson PE, Hu S, Yen YF, Robb F, Bok R, Schulte R, Xu D, Hurd R, Vigneron D, Nelson S. Multi-channel metabolic imaging, with SENSE reconstruction, of hyperpolarized [1-(13)C] pyruvate in a live rat at 3.0 tesla on a clinical MR scanner. *J Magn Reson.* 2011; 208(1):171–177. [PubMed: 21130012]
- Viale A, Aime S. Current concepts on hyperpolarized molecules in MRI. *Curr Opin Chem Biol.* 2010; 14(1):90–96. [PubMed: 19913452]
- Warburg O. On the origin of cancer cells. *Science.* 1956; 123(3191):309–314. [PubMed: 13298683]
- Ward CS, Venkatesh HS, Chaumeil MM, Brandes AH, Vancrickinge M, Dafni H, Sukumar S, Nelson SJ, Vigneron DB, Kurhanewicz J, James CD, Haas-Kogan DA, Ronen SM. Noninvasive detection of target modulation following phosphatidylinositol 3-kinase inhibition using hyperpolarized 13C magnetic resonance spectroscopy. *Cancer Res.* 2010; 70(4):1296–1305. [PubMed: 20145128]
- Wei LH, Su H, Hildebrandt IJ, Phelps ME, Czernin J, Weber WA. Changes in tumor metabolism as readout for Mammalian target of rapamycin kinase inhibition by rapamycin in glioblastoma. *Clin Cancer Res.* 2008; 14(11):3416–3426. [PubMed: 18519772]
- Witney TH, Kettunen MI, Day SE, Hu DE, Neves AA, Gallagher FA, Fulton SM, Brindle KM. A comparison between radiolabeled fluorodeoxyglucose uptake and hyperpolarized (13)C-labeled pyruvate utilization as methods for detecting tumor response to treatment. *Neoplasia.* 2009; 11(6): 574–582. 571 p following 582. [PubMed: 19484146]
- Workman P, Clarke PA, Guillard S, Raynaud FI. Drugging the PI3 kinome. *Nat Biotechnol.* 2006; 24(7):794–796. [PubMed: 16841064]
- Yang L, Clarke MJ, Carlson BL, Mladek AC, Schroeder MA, Decker P, Wu W, Kitange GJ, Grogan PT, Goble JM, Uhm J, Galanis E, Giannini C, Lane HA, James CD, Sarkaria JN. PTEN loss does not predict for response to RAD001 (Everolimus) in a glioblastoma orthotopic xenograft test panel. *Clin Cancer Res.* 2008; 14(12):3993–4001. [PubMed: 18559622]

Research Highlights

- We use hyperpolarized ^{13}C MRSI to monitor mTOR-targeted therapy in glioblastoma
- Hyperpolarized lactate-to-pyruvate ratio drop early following onset of treatment
- Tumor volume remains unchanged until late time points during treatment
- The drop in lactate-to-pyruvate ratio is associated with a drop in LDH levels
- Lactate-to-pyruvate ratio is an early biomarker of drug target modulation

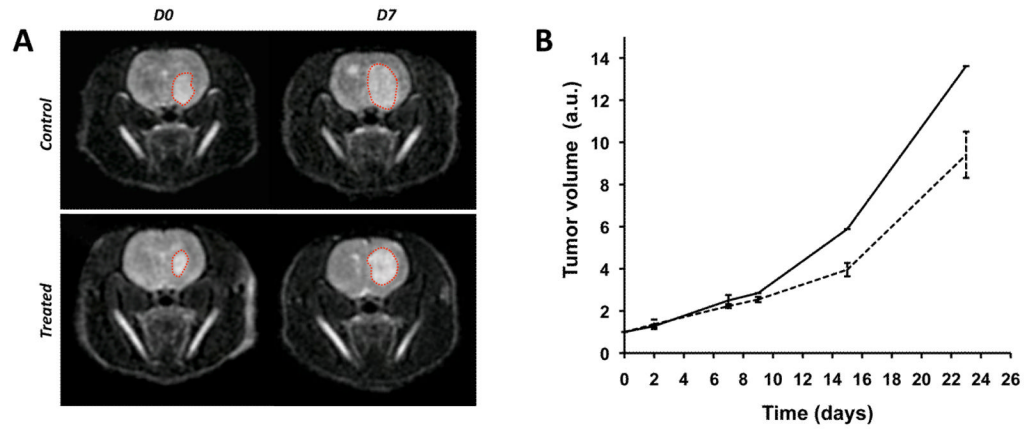


Figure 1.

(A) Axial T2-weighted images of one control (top) and one Everolimus treated (bottom) animal. The left column corresponds to data acquired prior to treatment initiation (D0), the right column to data obtained at D7. Orthotopic GBM tumors can be seen as hyperintense signals on the images (red dotted lines), illustrating tumor growth. (B) Tumor volume was assessed from anatomical images as a function of days of carrier/Everolimus treatment for both control (plain line) and treated (dotted line) groups, respectively. No changes in tumor volume are noticed between the two groups at D7. Slower tumor growth can be seen in Everolimus treated animals at later time points.

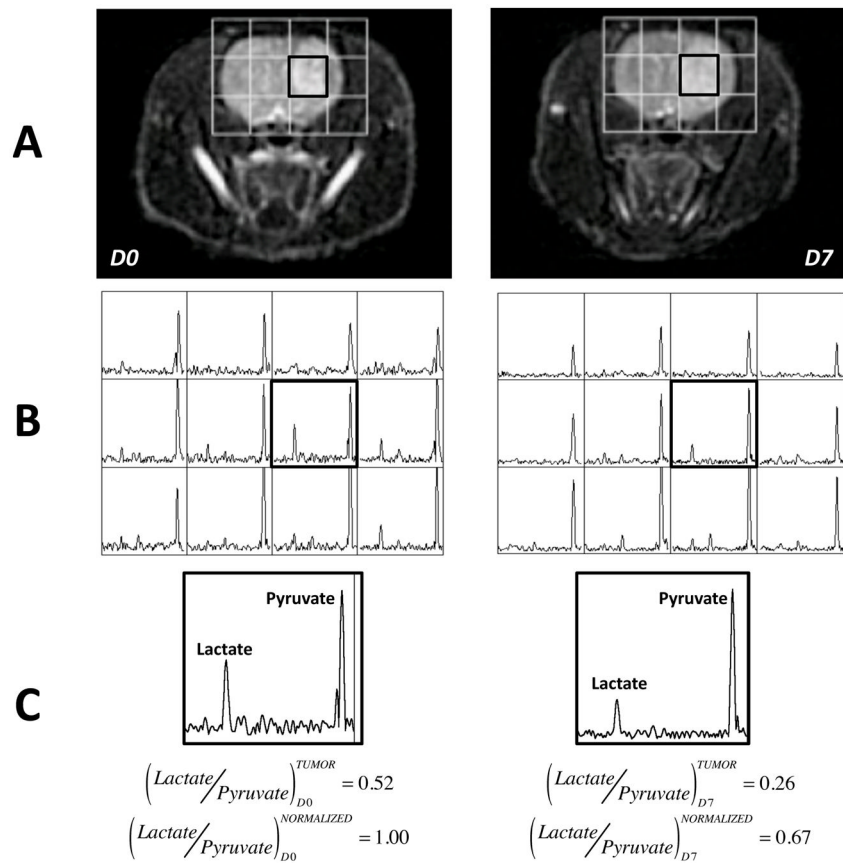


Figure 2. (A) HP ^{13}C MRSI grids superimposed to anatomical images acquired from one Everolimus treated animal at D0 (left) and D7 (right). The tumor voxels (>80% of tumor tissue) are presented as bold boxes. (B) Corresponding HP ^{13}C MRSI spectra. (C) HP ^{13}C spectra from the tumor voxels of interest and corresponding values of $(\text{Lactate}/\text{Pyruvate})_{D0}^{TUMOR}$ and $(\text{Lactate}/\text{Pyruvate})_{D0}^{NORMALIZED}$. A decrease in the $(\text{Lactate}/\text{Pyruvate})_{D0}^{TUMOR}$ ratio can clearly be observed after 7 days of Everolimus treatment.

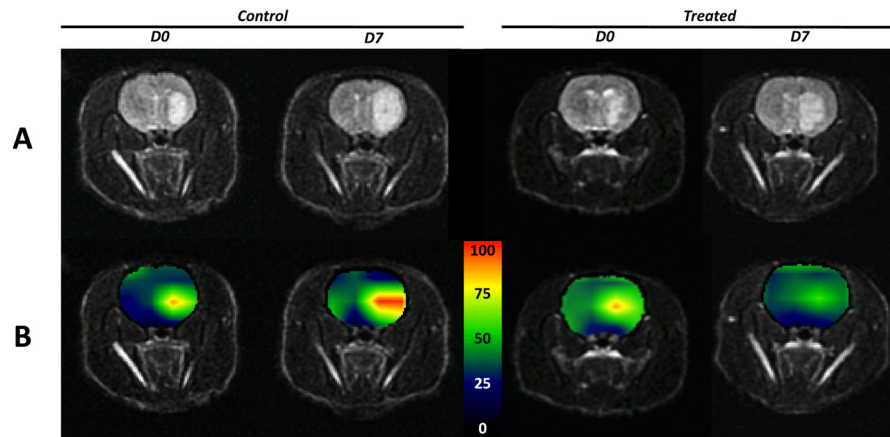


Figure 3. (A) Axial T2-weighted images and (B) corresponding heatmaps of the $(Lactate/Pyruvate)^{NORMALIZED}$ ratios derived from HP ^{13}C MRSI datasets of one control (left) and one Everolimus treated (right) animal. For each animal, the left column corresponds to data acquired prior to initiation of treatment (D0), the right column to data obtained at D7. Everolimus treatment induces a decrease of the $(Lactate/Pyruvate)^{NORMALIZED}$ ratio in the tumor region for the treated animal, whereas an increase of this ratio can be seen in the control animal.

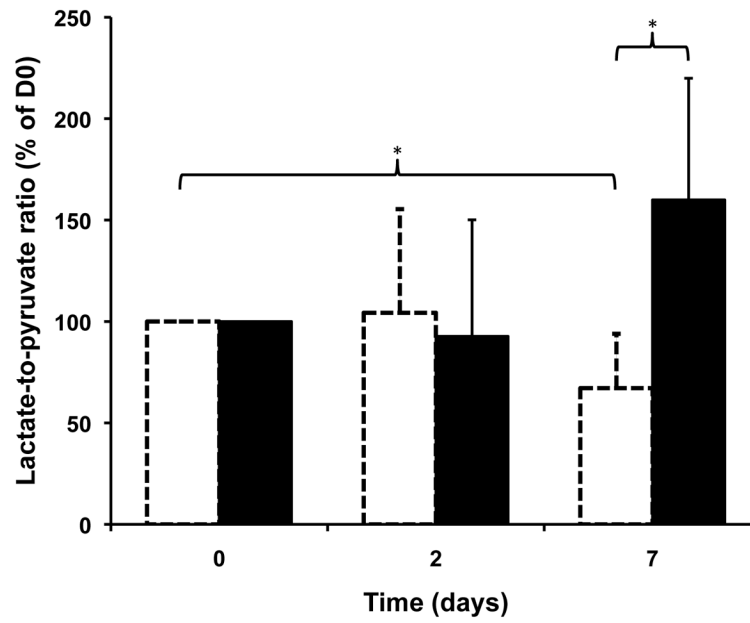


Figure 4. Histogram of the average ($Lactate/Pyruvate$)^{NORMALIZED} ratios at D0, D2 and D7 for control (black) and treated (white, dotted) groups. The average ratios were significantly different between control and treated animals at D7, and a significant decrease in this ratio was measured between D0 and D7 for the treated group. * $p=0.05$

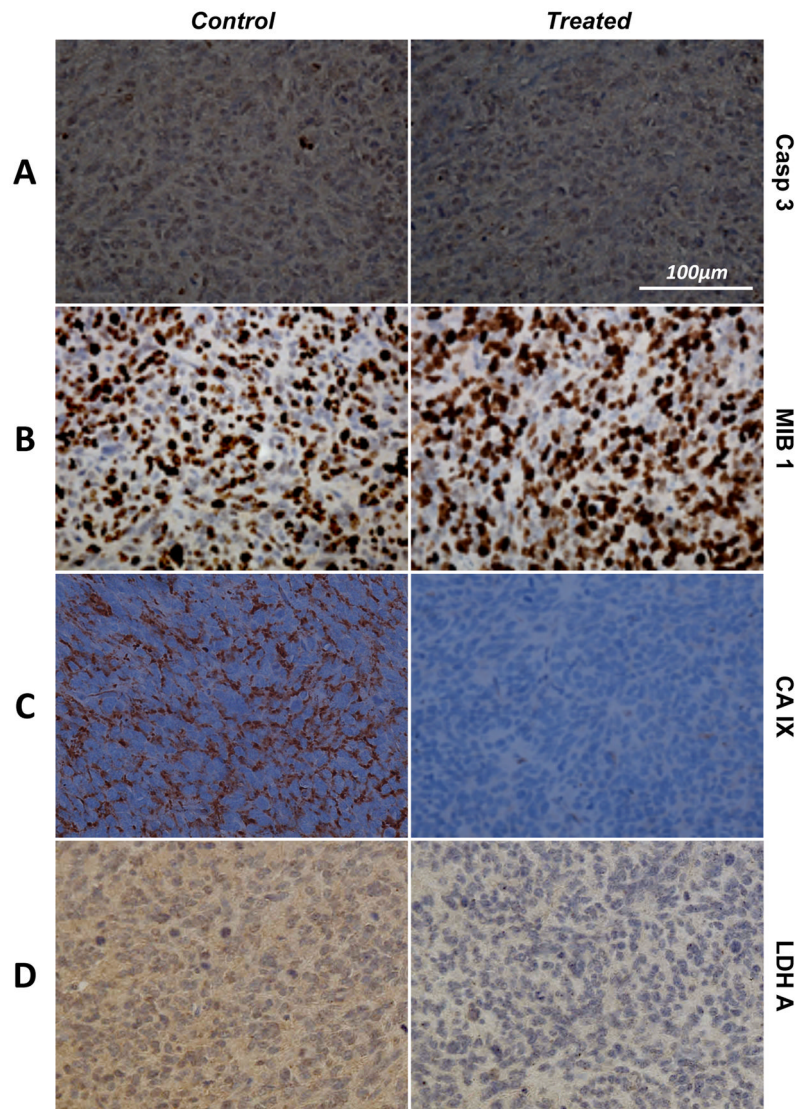


Figure 5. (A) Casp3, (B) MIB-1, (C) CA-IX and (D) LDH-A IHC stains of orthotopic GBM tumors resected after 7 days of carrier (left, control) and Everolimus (right, treated) treatments. No differences are observed between the two samples for both Casp3 and MIB-1, suggesting identical levels of apoptosis and proliferation, respectively. However, a clear drop CA-IX and LDH-A can be seen in the treated tumor.